Reprinted from JOURNAL OF PHYSICAL OCEANOGRAPHY, Vol. 21, No. 2, February 1991
American Meteorological Society

Vertical Structure of the Seasonal Cycle in the Central Equatorial Atlantic Ocean: XBT Sections from 1980 to 1988

G. REVERDIN,*,@ P. RUAL,** Y. DU PENHOAT** AND Y. GOURIOU‡

*LODYC, Paris, France
@Lamont-Doherty Geological Observatory, Palisades, New York
**ORSTOM, B.P. A5, Nouméa, Nouvelle-Calédonie
‡Centre ORSTOM, IFREMER, Plouzané, France

(Manuscript received 21 April 1989, in final form 13 August 1990)

ABSTRACT

A set of temperature profiles from expendable bathythermographs collected from 1980 to April 1988 along two ship routes transecting the equatorial Atlantic from 11°N to 11°S is analyzed to infer the vertical structure of the annual variability of the temperature and the currents in the upper ocean.

During the average seasonal cycle, the vertical isotherm displacements occur earlier below 300 meters than near the surface at most locations within 4 degrees of the equator. At the equator the amplitude of the displacements does not decrease with depth in the upper 500 meters. This still holds down to 700 meters, but there are less data at these depths. The lead of the deeper isotherm displacements with respect to those in the upper thermocline implies that there is a contribution to the pressure forces from these layers that is not in phase with the contribution of the upper thermocline. This also suggests that the energy source of the seasonal variability is close to the surface. Dynamic height and geostrophic currents relative to 400 db are also estimated. A seasonal cycle is found on the subsurface currents, which vary by up to a factor two during the cycle.

1. Introduction

Individual temperature sections across the Atlantic Ocean show a different structure between 10°N and 6°S than farther poleward, where the thermocline is spread over a considerable depth (Fig. 1). Usually near the equator, there is a surface mixed layer overlying a sharp thermocline extending to a temperature of 14°–15°C, which in turn overlays a layer of reduced vertical gradients, i.e., the thermostad. Still deeper, vertical gradients often increase around 300 m (temperature about 11°C), which we will refer to as the deeper thermocline, below which gradients are again reduced. In this paper, we wish to present data to quantify the variability below the upper thermocline.

Previous studies of the seasonal cycle in the equatorial Atlantic ocean suggest that there is a response in the upper thermocline related to the wind forcing (Merle 1980, 1983; Katz 1981; Garzoli and Katz 1983; Houghton 1983; Picaut 1983). Because these earlier observations were nonsynoptic, a field program (FOCAL-SEQUAL: Français Océan Climat dans l'Atlantique Equatorial-Seasonal Equatorial Atlantic program) was undertaken in 1982–84 in the tropical Atlantic Ocean to investigate the seasonal variability in relation to the wind field. The emphasis of the experiment was the upper-ocean dynamics, and measurements were concentrated in the upper ocean. However, bottom-mounted inverted echosounders (IES), which provide a bottom-to-surface acoustical time, have also been implemented for the study of the upper ocean. Before the experiment, a linear relationship was considered adequate to interrelate surface dynamic height, acoustical travel time, heat content, and the depth of the thermocline (Merle 1980; Katz and Garzoli 1982; among others). The FOCAL-SEQUAL mooring data have also suggested that the upper thermocline contributes to a large share of the near-surface dynamic height signal (Weisberg and Weingartner 1986).

However, at the equator at 4°W, during the upwelling seasons of 1983 and 1984, Houghton and Colin (1986) noticed that the upwelling near 300 meters (the 11°C isotherm depth) happens earlier than in the upper thermocline (20°C isotherm depth). This feature was not noticed in the average seasonal cycle (Houghton 1983), but at (4°50′N, 4°W) near the coast of Guinea, Picaut (1983) also found a lead of the deep isotherms in the seasonal cycle. These observations raise the question of how the variability below the upper thermocline may contribute to the dynamics of the upper ocean, and whether integrated signals, such as the travel time from IES are equivalent to upper thermocline characteristics (e.g., the depth of the 20°C isotherm).

To pursue the investigation of the deep variability suggested by these observations, moored records of temperature and currents would be most appropriate.

Corresponding author address: Dr. Gilles Reverdin, Lamont-Doherty Geological Observatory, Palisades, NY 10964

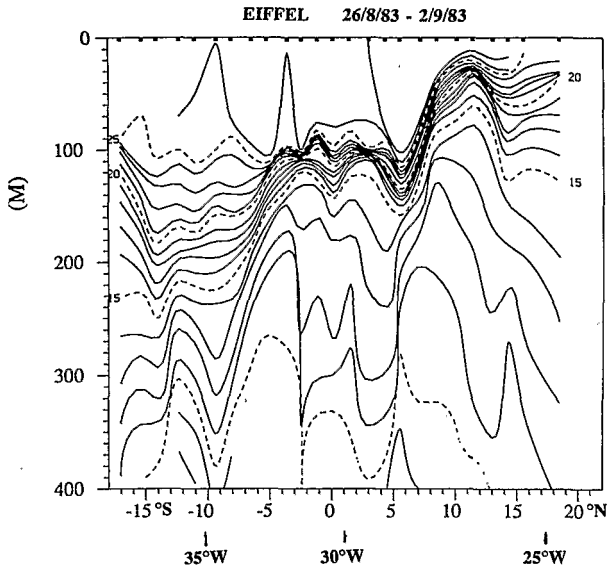

FIG. 1. A temperature section in August 1983 performed by the vessel *Eiffel* along the route from Europe to Brasil (western route).

However, not enough records of sufficient duration are available at depth. Hence, the present study is based mainly on expendable bathythermograph casts (XBT) collected along two routes (Fig. 2) between 1980 and 1988. The western section was started in mid-1980, and monitored by the Deutsche Hydrographische Dienst in Germany (DHD), and by the French ORSTOM (*Institut de Recherche Scientifique pour le Développement en Coopération*). Ancillary data have been added, including CTD and XBT casts from the programs in 1982–84. The data and an analysis up to early 1983 of the upper layers are presented in Rual and Jarrige (1984) and up to 1985 in Emery et al. (1987). The eastern route was first implemented for the SEQUAL field program (Bruce et al. 1985), and since 1986 it has been maintained as a TOGA XBT line. However, the sampling is less dense than on the western route.

Before presenting the analyzed time series, we will briefly outline our approach. The analysis technique used to construct time series of temperature and isotherm depths is presented in appendix A. Dynamic height is computed from these analyzed temperature profiles, using an average seasonal relationship between T and S estimated from hydrographic data collected after 1980. Geostrophic currents perpendicular to the XBT lines are then evaluated in the open ocean (the western line runs close to Brasil south of 6°N, and the eastern line runs close to Africa north of 6°N). A discussion of the geostrophic approximation and a comparison with measured currents at 6°N, 3°N and 1°44′N along 28°W is also given in appendix B. The estimated geostrophic currents seem to reproduce well the near surface variability except within 1.5° lat of the equator, but does not reproduce the subsurface variability. This latter mismatch is unfortunate, but both badly sampled high frequencies and the location of the moorings close to boundaries of the subsurface currents could explain this, so that it does not a priori imply a flaw in the methodology.

Since currents primarily flow along isopycnal surfaces, there is the possibility at a fixed depth to encounter a variability related solely to the vertical advection of the current structure. This advection was shown to be important for the equatorial undercurrent from mooring data at 24° and 26°W (Weisberg 1985) and at 28°W (Weisberg et al. 1987). Therefore, we chose to present the estimated geostrophic velocity on temperature surfaces rather than at fixed depth.

We constructed an eight-year time series on a 1.5° latitudinal grid. A composite seasonal cycle was then constructed from these eight years, and the uncertainty in this average was computed by assuming that the eight individual years provide independent Gaussian-distributed realizations of the seasonal cycle. This dataset was not adequate to resolve high frequencies, e.g., the signals associated with equatorial Kelvin waves or the set-up of the upwelling in the Gulf of Guinea. The low frequencies included in the analysis have periods longer than three months. This filter retains a significant share of the total oceanographic variability in the tropical Atlantic. For example, the low-pass filtered time series of 20°C isotherm depth from a mooring at (0°, 4°W) in 1983–84 had 79% of the variance of the daily record.

Our analysis focused on the seasonal variability of the temperature and geostrophic currents near the surface and in the deep thermocline. The datasets available had several limitations.

First, the two XBT lines do not intersect the areas of largest variability, which according to climatological study are found further west and in the equatorial Gulf of Guinea. Interannual anomalies in 1984 were much larger in the eastern Gulf of Guinea than at 10°W (Hisard and Hénin 1987).

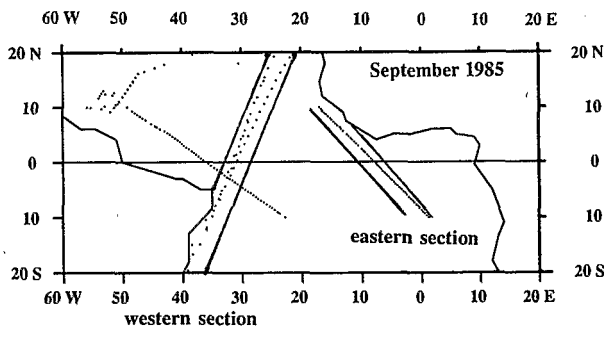

FIG. 2. An example of the monthly distribution of profiles in the tropical Atlantic ocean. The two investigated XBT lines (west and east) are bounded by the straight lines drawn.

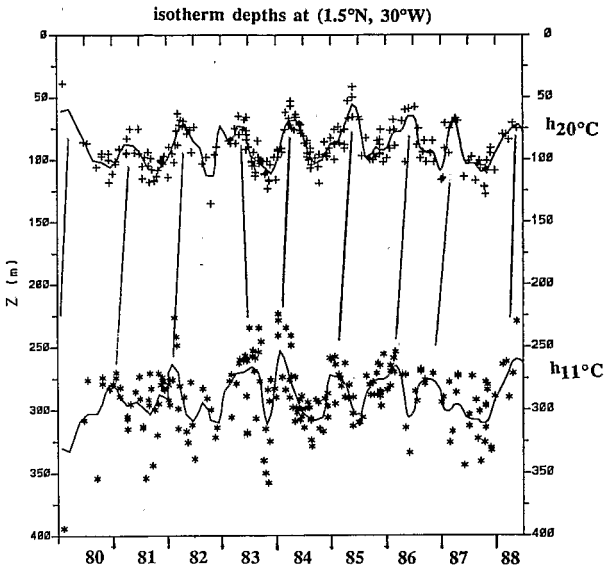

FIG. 3. Time series of the 20°C isotherm depth and of the 11°C isotherm depth at (1.5°N, 30°W) along the western route constructed from 240 profiles with an objective analysis routine filtering out periods less than 3 months. The crosses correspond to the individual measurements which depart from the analysis with a rms of 8 m for the 20°C isotherm and 20 m for the 11°C isotherm. For 1983–84, two well-sampled years, the resulting uncertainty in the analysis is of the order of 3 m for the 20°C depth and 10 meters for the 11°C depth. The lines connect the ridges in the two curves.

Second, there was considerable scatter in the measurements; e.g., Fig. 3 shows two isotherm depths at 1.5°N along the western route (Fig. 3). These isotherms suggest a seasonal cycle in both the upper and deep thermocline. In the upper thermocline (the 20°C isotherm curve) the noise level is low, and year to year differences are significant. However, in the lower thermocline, which is our main concern here, the noise level is much larger, and for the 11°C isotherm depth, the error bars estimated from the dispersion of the data with respect to the low frequency signal are of the order of 7 m, which encompasses most of the year to year differences (Fig. 4a for the eastern route). Thus, the data are not adequate to study the interannual variations. This is even more true for the estimated geostrophic currents (Fig. 4b). However, for the isotherm depths, and even for the deep geostrophic currents, these figures suggest a seasonal cycle.

2. The seasonal variability

a. The average seasonal cycle of isotherm displacements

The average seasonal cycle will be discussed along the two routes for an isotherm depth in the upper thermocline (20°C) and one in the lower thermocline (11°C). The residual rms error estimated from the

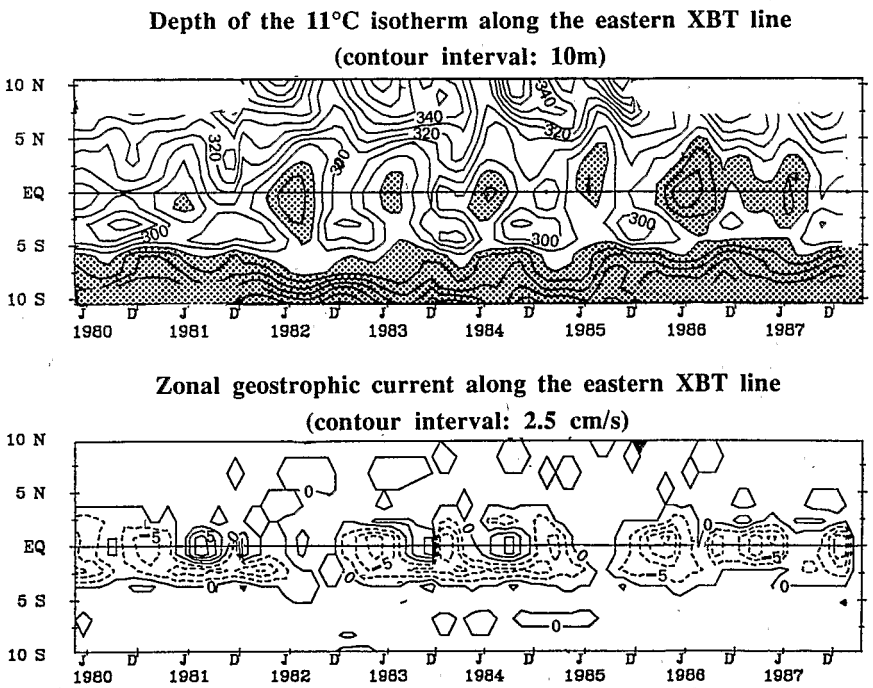

FIG. 4. Time series of the 11°C surface along the eastern section (1.5° grid). (a) The depth of the surface (shaded for depth less than 280 m); (b) The estimated geostrophic currents. The analysis north of 9°N and south of 9°S in 1980, 1981, 1986, 1987 is not presented, as it is too uncertain because of a sparcity of profiles.

year-to-year differences is about 2 meters for the 20°C isotherm and 4 to 5 meters for the 11°C isotherm. However, it varies from month to month, mainly because of the data distribution. The maximum rms error for the depth of the 11°C isotherm is 11 m in August at 12°N in the west. The seasonal signal is highly significant along both lines. In this average seasonal cycle, the annual harmonic accounts for more than 80% of the variance, except along the eastern route, north of 4°N, where semiannual variability is also large, and between 7°S and 10°S where variability is small.

In the places where the annual harmonic dominates, it is justified to illustrate the signal by selecting the amplitude and the phase of the annual harmonic, and this is summarized on Fig. 5, comparing the 20°C depth and the 11°C depth, where we have adopted a finer meridional resolution of 0.5° to compare an average seasonal cycle between 10°N and 10°S.

The variability in the upper thermocline close to the western route has already been described from other sets of data: between the equator and 10°N by Garzoli and Katz (1983), farther north, by Stramma and Siedler (1988). Our results (Fig. 5a), as well as Emery et al. (1987) for a subset of the data, support these earlier studies. The largest seasonal displacements are found at 4°N with a secondary maximum at 3°S. Variability is smaller south of 3°S than farther north. At 9°N and 8°S, variability is minimum, and seasonal displacements further poleward at 12°N and 14°S have the opposite phase. On the eastern route (Fig. 5b), the 20°C isotherm has a maximum variability at the equator and a minimum variability at 3°N. We should also comment that at the equator the annual harmonic only includes 80% of the variance. This is caused by the intense upwelling event peaking in June–July, which does not last long.

On Fig. 5b, along the eastern route, it can be seen that the depth of the 11°C isotherm has a different annual signal than the 20°C isotherm depth. There, the variability of the 11°C isotherm is dominantly explained by the annual harmonic, and its largest variability is located off the equator.[1] Along the western route, there is a broad area of large variability in the 11°C isotherm depth between 2°S and 6°N, instead of the maximum found at 4°N in the 20°C isotherm depth. In the west, the phase of the signal is also different for the 11°C depth than for the 20°C depth, with a lead of the 11°C depth of the order of 2 to 4 months between 3°S and 6°N and 1 to 2 months north of 10°N. The uncertainty on the phase at the 11°C depth is of the order of 10 days, therefore, it is not possible to assess whether the phase differences between the equator and 3°N or 2°S are significant. On the other hand, 5°N lags the other equatorial latitudes (Fig. 5a). Near the equator along the eastern route (close to 10°W), the lead is not as clear, where the maximum uplift occurs almost at the same time for the 11°C isotherm and for the 20°C isotherm. These characteristics for the analysis of the annual harmonic are also found in individual years: the near-equatorial heat content on the western route presented in Fig. 6 suggest a different phase below 300 meters than the upper layer heat content (discussed for the average climatological seasonal cycle in Merle 1980), at least for 3 of the four presented years; for 7 out of the 8 years of the time series of the 11°C isotherm depth at 3°N (on Fig. 3), the peaks and troughs occur earlier than in the upper layer.

b. Vertical structure of isotherm displacements

To illustrate the vertical structure of the variability, profiles for the annual harmonic are shown at various latitudes close to the equator along the western route (Fig. 7a–7d). At these latitudes, the phase decreases with depth, at least down to 700 meters, so that the deeper isotherms lead the shallower isotherms. The uncertainty in the phase (estimated by subsampling the time series) is of the order of 5 days in the upper thermocline, but increases to 10 days at 300 meters, and is of the order of 20 days at 500 meters. Thus, phase change with depth is still significant. The constant phase between 200 and 600 m at 2°S, and from 350 to 600 m at 5°N is probably significant. In the upper thermocline, the largest variability is observed at 3°N, but decreases sharply between 200 and 250 meters. Below 300 meters, the amplitude is larger at the equator than at other latitudes, and it is larger there than closer to the surface. The uncertainty in amplitude is of the order of 1 meter in the upper thermocline, but increases to 2 meters below 300 meters, and some of the other details in the profiles are not significant.

Along the eastern route (Fig. 7e–7f), large variations of the phase with depth are also found, which at the equator are corroborated by mooring data in the upper 500 meters at (0°, 4°W) (including unpublished data from the CIPREA moorings in 1978–80). In the upper thermocline and the thermostad, the signal varies strongly with latitude, and it is only below 250 meters that the upward phase speed is well defined within 4° of the equator.

[1] The 4°W composite seasonal cycle (see also Houghton (1983) and Picaut (1983) for different years) shows characteristics not too different from those of the eastern route. The timing of the shallowest equatorial 20°C isotherm depth is a month later than in our eastern route analysis (located 5° to the west), a difference not found at larger depths. The largest variability for the 11°C depth is located near 2°N–3°N and at 2°S, and not at the equator like in the upper thermocline. It was also found by Houghton (1983) that the equatorial trapping of the upwelling is confined above 200 m. For two well sampled individual years 1983 and 1984, the deep vertical displacements are also stronger at off-equatorial latitudes (Houghton and Colin 1986), and at the equator, the shoaling of the 11°C isotherm occurs a month earlier than in the upper thermocline.

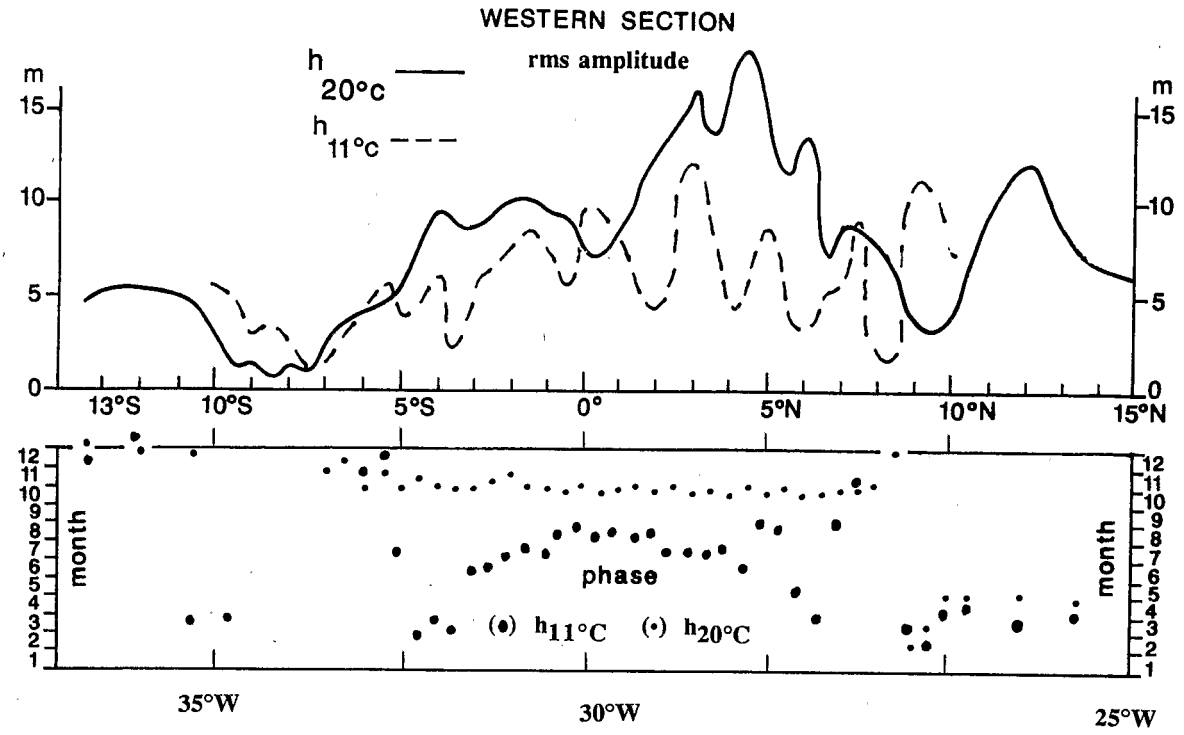

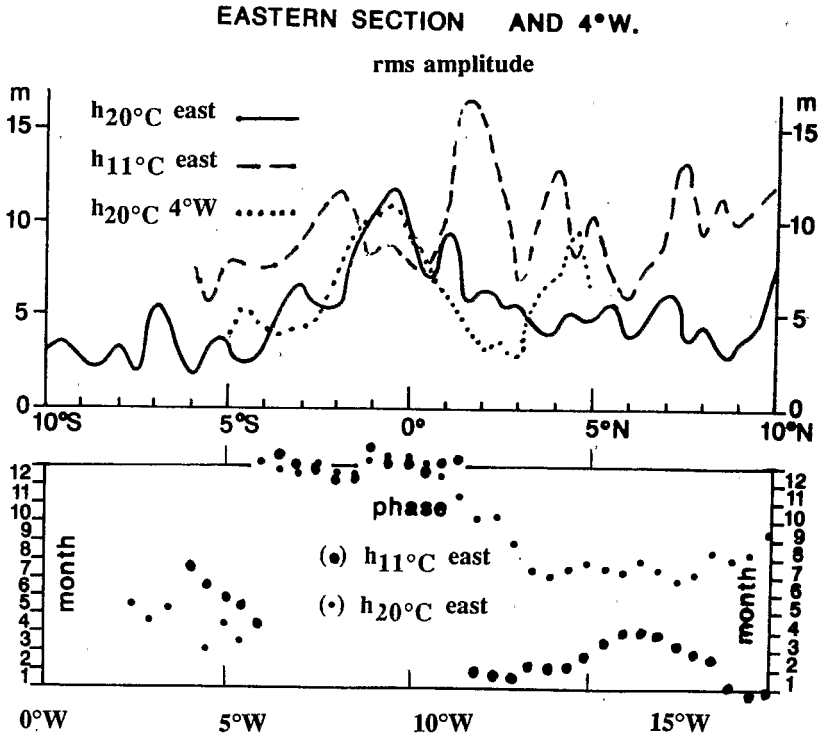

FIG. 5. Standard deviation (m) and phase (months) of the annual harmonic of vertical displacements for two isotherm depths (20°C, continuous line and 11°C, broken line) on the western (a) and eastern (b) sections (both, latitude and longitude are indicated along the abcissa). The phase indicates when the greatest depth of the isotherm is attained (in months), and we omit the phase when the amplitude is low compared to the interannual deviations. Between 10°N and 10°S, a 0.5° latitude grid is used, and further poleward the 1.5° grid. On Fig. 5b, we also indicate the amplitude of the annual harmonic of the 20°C isotherm depth displacements along 4°W (mixed line).

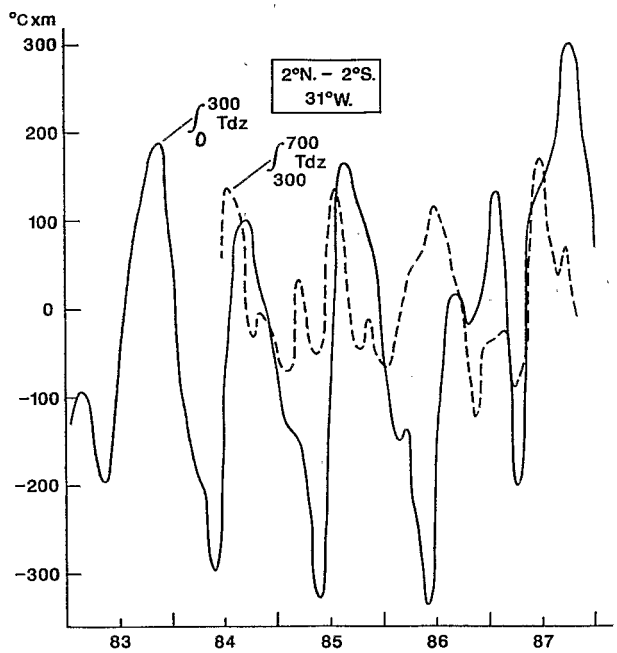

FIG. 6. Heat content estimated in two layers from a mixed data set of CTD casts and XBT profiles near the equator (2°N–2°S). One layer extends between 0 and 300 m, the other between 300 and 700 m, and arbitrary constants have been substracted from the two curves. The upper heat content is composed from a large number of profiles (749), and uncertainties are of the order of 10°C m, and the lower heat content is composed from 140 profiles with typical error bars of ±30°C m. The months with profiles included in both curves are indicated by ticks on the lower axis.

The temperature variability below 300 meters contributes to changes in the heat content (Fig. 6) and dynamic height (Fig. 8). At the location shown in Fig. 8, the signal amplitude reaches 0.9 dyn cm for the layer 400–700 db compared with 5.1 dyn cm for the layer 50–400 db, which encompasses the upper thermocline. Further investigations on the respective importance of these layers for the dynamic height and the acoustical travel time measured by IES are given in appendix C.

The local potential energy associated with the seasonal displacements is evaluated as: $E_p = 0.5\rho N^2 \delta h^2$ where δh is the standard deviation of the vertical displacements, and N, a representative Brunt–Väisälä frequency for the annual average. If δh is a constant over a layer spanning a potential density range of $\Delta\sigma$, then $\int E_p dz = 0.5 g \Delta\sigma \delta h^2$. Along the equator, both at 4° and 28°W this suggests that the vertical displacements in the layer between 300 and 700 m contribute to a potential energy of the order of 20% of the seasonal potential energy in the upper 300 meters.

c. *Zonal geostrophic currents*

We rely on a 0.5° gridded analysis of the seasonal cycle in order to resolve the currents. The average current structure corresponds to what is known of the circulation, with alternating narrow eastward and westward flows. We will now investigate the seasonal cycle in the currents. The zonal currents are integrated vertically over three layers based on the vertical structure

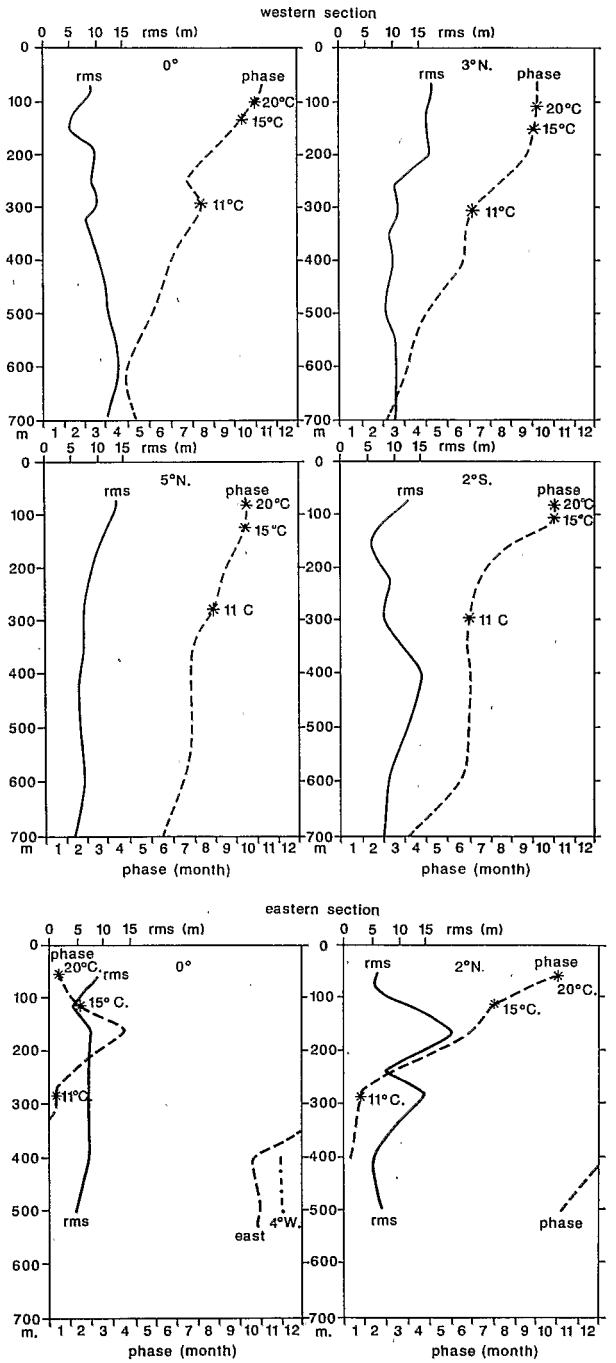

FIG. 7. Vertical profiles of standard deviation (m) and phase (refers to the date of the warmest temperature, dotted line in months) of the annual harmonic of the vertical displacement in various places along the western section (a to d) and the eastern section (e and f). In (e) the phase along 4°W is also indicated at 400 and 500 m.

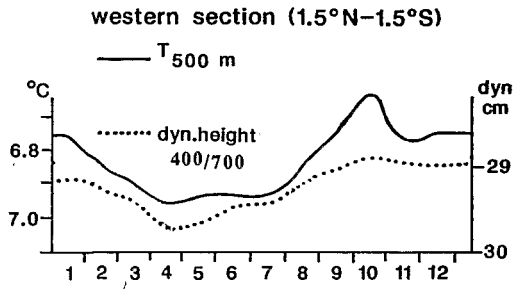

FIG. 8. Average seasonal cycle between 1.5°N and 1.5°S along the western route of the dynamic height between 400 and 700 db (dotted line) as well as the temperature at 500 m (full line).

in temperature sections (Fig. 1) to correspond to 1) the upper thermocline between 25°C and 15°C, 2) the thermostadt between 15° and 12°C, and 3) the lower thermocline between 12°C and 400 m.

The vertically integrated currents are then smoothed in latitude by a 1° running average, and then a (¼, ½, ¼) filter is applied in time on the monthly time series. The meridional boundaries between eastward and westward currents are first determined from these fields, and the zonal transport for each current is estimated. These zonal currents are indicated on Fig. 9. Near the equator, boundaries have been set at 1.5°S and 1°N, close to where the current is expected to change sign according to the meridional pressure gradient depicted on Fig. B1. In the east the northern boundary of the North Equatorial Countercurrent (NECC) is ill-defined, and has been set to 5°N.

Based on the average seasonal cycle (Fig. 9), the individual currents can be found throughout the year, and their latitudinal seasonal displacements are small (less than 1°) in the lower thermocline (Fig. 9c and 9f). Even in the upper thermocline, meanders are not pronounced. In the east, however, the SEUC width changes significantly, although 4°S is always within this eastward flow (the upper layer extends to the surface between June and October, and then the real current will strongly differ from the geostrophic estimate). The northern boundary of the western NECC also moves significantly, and it extends farther north between July and November.

The transports of the currents relative to 400 db do change seasonally (Fig. 9), typically within a factor of 2, but it is difficult to ascertain the uncertainties on this composite constructed from the 0.5° bin averages (the uncertainties indicated in the right margin of Fig. 9 result from a rough estimate of the uncertainty on individual monthly estimates of dynamic height on the 0.5° grid). Usually, the variability is above the rms uncertainty, except at the equator. The eight year time series in 1.5° bins (Fig. 4b) also suggest that near the equator the seasonal cycle is barely above the noise level. The variability is often annual, except in the thermostadt within 3° of the equator where it also has a semiannual component. The variations in the near-equatorial currents at depth appear to lead the upper thermocline ones, but this is probably within the uncertainty of the analysis.

The seasonal variability in other currents is well defined, even at subsurface. The deep SEUC in the east is weakest in July to September (geostrophic current relative to 400 db), a feature also found on individual fine resolution sections in 1980–85 (Bruce 1987). It is strongest at that time in the west. The NECC in the upper thermocline extends farther north between July and November, so that its transport peaks at a different time in this layer than in the two other layers, where changes in the meridional extension of the currents are less. The cycle that we find for the NECC in the two deep layers contrasts with the weak seasonal variability at 28° W argued by Cochrane et al. (1979). However, the seasons selected for the averaging in Cochrane et al. (1979) are February to April and July to September, and Fig. 9 suggests that they are not adequate for the deepest layers, because the maximum transport occurs in May–June and the minimum transport in December–January.

3. Discussion

In the deep thermocline we have found evidence for a large level of potential energy associated with the seasonal variability. If the seasonal vertical displacements were also present deeper in the ocean, these deep levels could contribute to a significant share of the seasonal potential energy of the water column. We have also noticed a seasonal variability in the zonal currents. It would be interesting to compare potential energy with the kinetic energy associated with the seasonal cycle; however, due to the large uncertainties on the analysis of the currents our estimate of the kinetic energy is not reliable, especially at the equator where we expect kinetic energy to be large.

Another suggestion for a seasonal variability of the equatorial currents is provided by the analysis of the dynamic height referred to 400 db. Our analysis shows near 300 meters a significant seasonal cycle of the zonal pressure force between the two tracks. The time integration of the pressure force is in phase with the analyzed geostrophic current (Fig. 10 where both terms have been averaged between 1.5°N and 1.5°S). This suggests that the currents at these depths are generated by the horizontal pressure forces. This of course is based on numerous assumptions, one being that the average of the estimates of the equatorial current from the two tracks is representative of the average in the area between the tracks.

Current meter mooring records at 300 meters on the equator also exhibit variability on seasonal time scales. At (0°, 4°W) sparse mooring records at 300 m (1978–1980 and 1984; Colin, personal communication) sug-

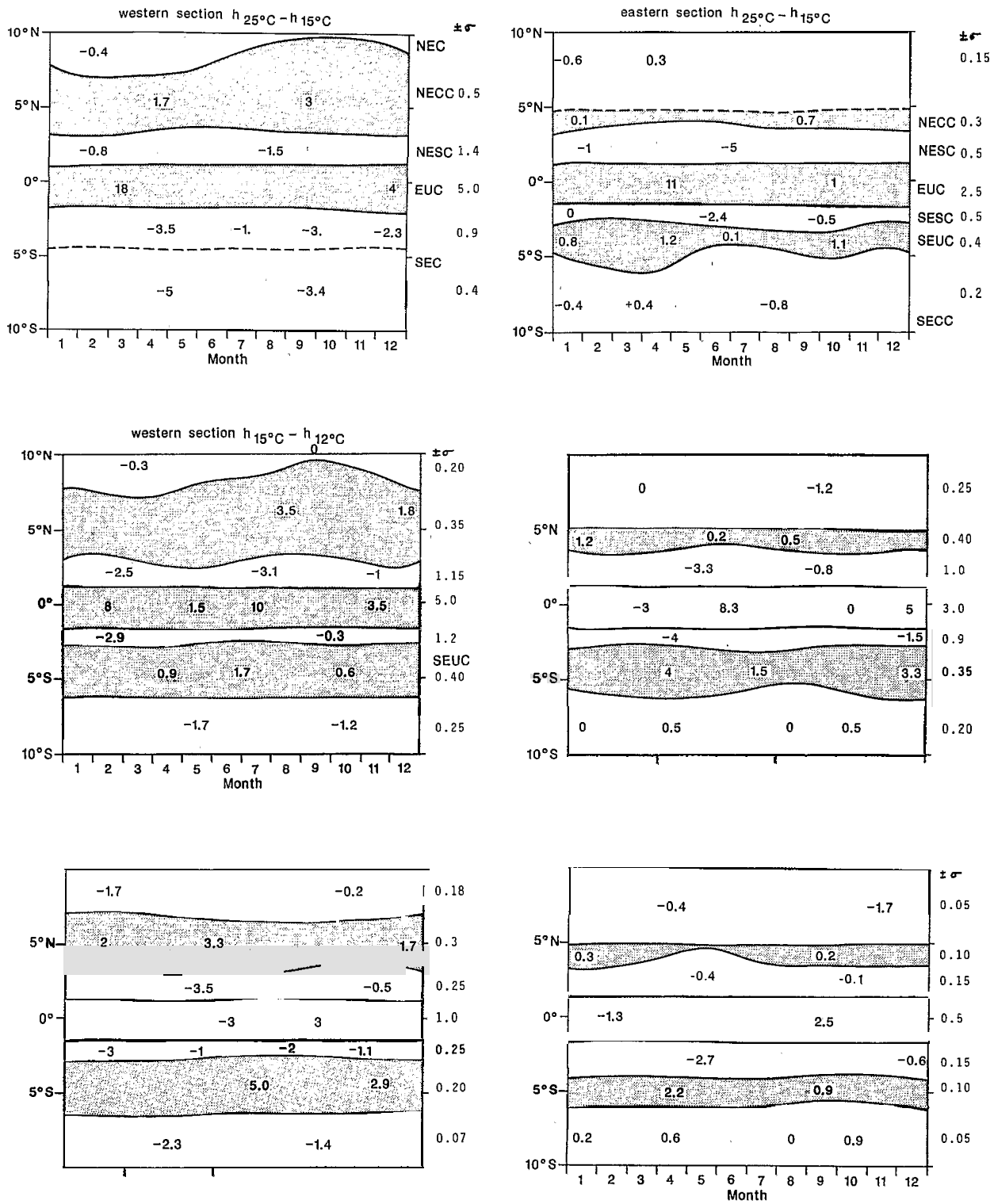

FIG. 9. Seasonal cycle of the currents in three layers (the upper thermocline, the thermostadt and the lower thermostadt) for the two sections from the 0.5° analysis. The cross-line currents are converted into zonal currents, assuming no meridional component. The currents are: North Equatorial Current (NEC), North Equatorial Countercurrent (NECC or NEUC), North and South branches of the Equatorial subsurface current (NESC and SESC), Equatorial Undercurrent (EUC), South Equatorial Undercurrent (SEUC), South Equatorial Current (SEC) and South Equatorial Countercurrent (SECC). Meridional boundaries of the currents and extrema of the transports are indicated (in Sverdrups; 1 Sv $\equiv 10^6$ m^3 s^{-1}). Arbitrary boundaries have been set at 1°N and 1.5°S to isolate the strong equatorial transports. In the right margin, an estimate of the uncertainty ($\pm$ one standard deviation in Sv) is given.

gest a seasonal cycle, as do measurements at 24°–28°W in 1974, 1981 (Weisberg 1985) and 1983–84 (Weisberg et al. 1987), both with westward flow in January–April and eastward flow in June–September. This is similar to the geostrophically estimated current with a reference at 400 db (Fig. 9 or Fig. 4). However, this agreement could be coincidental as current meter records at 500 meters also show large currents (with the opposite sign to the currents at 300 m). Thus, the currents at 300 meters could differ noticeably from currents relative to 400 meters such as we have computed. Also, there are hints for a large interannual variability at these depths from records at 590 meters and 680 meters on moorings placed at (0°, 4°W) in January 1977–June 1978 (Weisberg and Horigan 1981). Therefore, the available mooring time series are probably too short to construct a reliable seasonal cycle and estimate its kinetic energy. From the records, it seems however that at 300 meters at 4°W, the seasonal cycle rms variability should be of the order of 0.1 m s^{-1} or less, which corresponds to a kinetic energy of 0.5×10^{-2} m^{-2} s^{-2}, a value of the same magnitude, but smaller than the potential energy of 1.5×10^{-2} m^{-2} s^{-2} (for the particular years 1983 and 1984, Houghton and Colin (1987) find a larger potential energy of 2.5×10^{-2} m^{-2} s^{-2}).

From previous modeling studies, the main source of the seasonal energy in the equatorial Atlantic is the wind stress at the sea surface. Therefore, the spatially averaged energy fluxes are expected to be downward. The observed phase shifts with depth of the vertical displacements imply that at a given depth, dynamic height is not in phase with vertical displacements. This is usually interpreted as an indication that there is a flux of energy (downward if the deeper displacements occur earlier). This arises from the equation governing the Lagrangian rate of change of the sum of potential and kinetic energy, E, approximately written as

$$\frac{DE}{Dt} = -\mathrm{div}(\mathbf{u} \cdot P) - d(u \cdot \tau)/dz$$

where we have neglected the effect of horizontal diffusion by eddies, and τ is the vertical Reynolds stress (implicitely, all terms are averaged over a seasonal cycle). The first term on the right hand side is the rate of working of pressure forces (we will refer to $\mathbf{u} \cdot P$ as the working flux), and the second term is related to sources and sinks by vertical small scale motions. It is the vertical component of the working flux which is considered, and more specifically its seasonal component $w_s \cdot P_s$. To crudely estimate its magnitude, w_s is estimated as $\partial h/\partial t$, where h is an isotherm depth, and pressure is referred to 400 db (a shallow reference common to the two sections: an unfortunate choice required by the lack of deep data at most latitudes; if we had been able to select a deeper reference level (for example, 700 db), $w_s \cdot P_s$ would probably have been larger).

In most places, the estimated working flux is downward between 3°S and 9°N (positive values in Fig. 11 where the eastern and western sections are averaged to suggest the mean values in the central equatorial Atlantic). The exception is near the equator on the eastern route between 20° and 15°C (not shown); of course, this could be related to a deviation from the relation $w = \partial h/\partial t$, as the 20°C isotherm gets very close to the surface during the upwelling season. The mean flux on the 11°C horizon averaged between 3°N and 3°S is 0.15×10^{-6} W m^{-2}, which is 10–15 times smaller than close to the surface. The uncertainty on estimates for individual latitudinal bins is of the order O(1), so that this average is significantly nonzero, but it strongly depends on the reference depth. For comparison, the wind stress seasonal energy input is estimated from $u_{gs} \cdot \tau$, where $\mathbf{u}_{gs}$ is the mixed-layer geostrophic velocity (annual average removed), and τ is a seasonal zonal wind stress estimated from ship reports for each of the two sections during 1982 to 1984. The energy input averaged between the two routes suggests a maximum near the equator of 1.5×10^{-6} W m^{-2}, with a secondary maximum of the order of 0.6×10^{-6} W m^{-2} at 8°N. Notice that these magnitudes are comparable to the downward energy flux in the upper thermocline, but are larger than the flux in the lower thermocline. However, we know that equatorial waves will also carry energy horizontally away from the source region, and

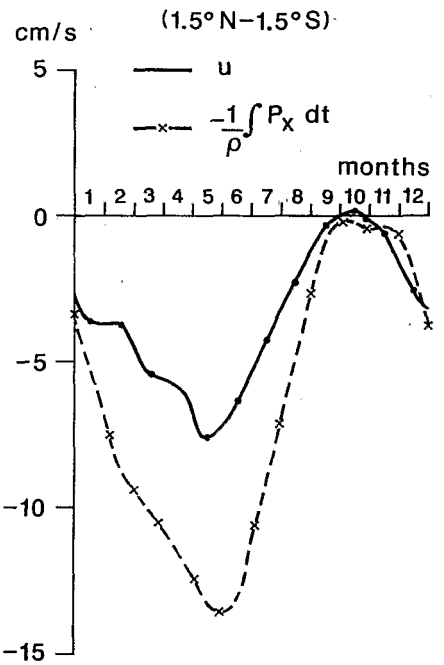

FIG. 10. The average seasonal cycle between 1.5°N and 1.5°S of the zonal current (the mean of the western and eastern routes) and the time integral of the zonal pressure force between the two tracks are presented at the 11°C isotherm level.

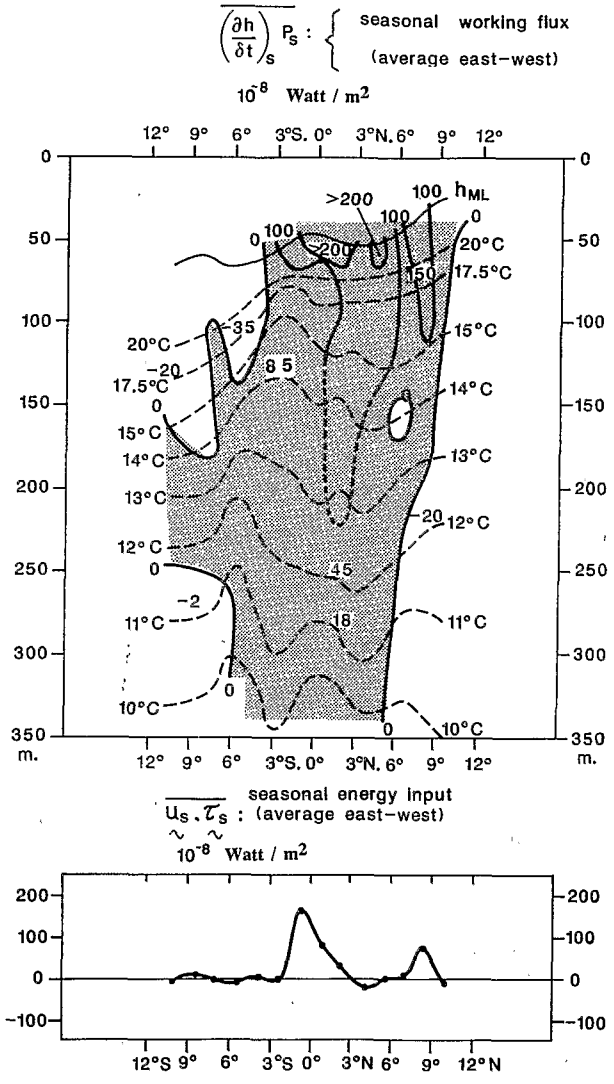

FIG. 11. Fig. 11a, the estimated vertical flux of energy by the pressure force averaged between the two sections (reference for pressure is 400 db). Fig. 11b, the seasonal energy input by the wind (an average of the two sections).

that we therefore do not expect a local relationship between the wind input and the downward energy flux. An example is at 8°–9°N where the energy input at the surface is large, but where there is no downward energy flux below 100 meters. However, a more careful investigation of the energy budgets requires both a spatial coverage of the tropical Atlantic, and a deeper reference level than could be achieved here.

We should also emphasize the differences in the isotherm vertical displacements between the eastern and the western sections which were shown, for example, in Fig. 5. They imply that the seasonal horizontal pressure force between the two sections (not shown) peaks off the equator, and that oscillating meridional velocities are present. Also, because the meridional and vertical structure of the variability is different at the two longitudes, this variability between 100 and 500 meters cannot be interpreted as a single vertically propagating wave. Considering the small fetch of the equatorial Atlantic, it is not surprising that the response at the low frequencies takes place on the basin scale, and invokes in the equatorial band both Kelvin and Rossby waves [various modeling studies have discussed this issue, such as Cane and Sarachik (1981), Busalacchi and Picaut (1983), McCreary et al. (1984), Philander and Pacanowski (1986), Weisberg and Tang (1987) or du Penhoat and Tréguier (1985)].

4. Conclusions

The analysis of eight years of temperature profiles along the two XBT routes in the central tropical Atlantic Ocean has provided a new insight on the variability in the upper 700 meters. In the upper thermocline, interannual deviations are not large compared to an average seasonal cycle (1980–88). This average is similar to earlier descriptions of the seasonal cycle in the upper thermocline (Merle 1980, 1983; Katz 1981; Houghton 1983; among others). In the lower thermocline, it is not possible to quantify interannual deviations since uncertainties are larger, due to the fewer data and their larger errors. It should be noted that the investigation does not include the areas where the largest seasonal variability is found in the upper thermocline; i.e., west of 30°W north of the equator and in the equatorial Gulf of Guinea (Merle and Arnault 1985; Garzoli 1987; Katz 1987). It is probable (as was observed in 1984) that interannual variability may also be smaller along the ship-of-opportunity routes.

In this analysis of a composite year, the seasonal variability of the lower thermocline within 5° of the equator differs from the variability of the upper thermocline. The annual harmonic does not have the same meridional structure or phase in the two layers. Near the equator, the 400 to 700 db layer could contribute to a peak-to-peak seasonal pressure signal of 1 dyn cm, compared to typical signals between 0 and 400 db of the order of 10 dyn cm. The question should be raised on whether we can neglect the deep variability for investigations of the upper ocean. For example, one can argue from these results that reduced gravity models cannot be very satisfactory in reproducing the seasonal cycle of sea surface level near the equator or in simulating the changes in the meridional slope across the North Equatorial countercurrent (notice however that north of the current, the variability is nearly in phase across the sampled water column). This could be even worse with IES travel times used as records as indicators of sea level (these records are more sensitive to the deep layers, cf. appendix C).

The zonal current relative to 400 db was estimated geostrophically for a composite year from a pressure distribution on a 0.5° meridional grid. This grid does smooth the currents boundaries, because of the small width of the currents. However, below the upper thermocline, only small meridional seasonal shifts of the currents are found. The off-equatorial seasonal variability estimated for the composite year is large, but is not associated with seasonal reversals of the flow. Also, it is known that the off-equatorial flows extend deeper than 400 db (Cochrane et al. 1979; Molinari 1982; among others), and that the reference to 400 db is therefore not the most appropriate. However, currently, the XBT routes are sampled each month with no more than by 1 profile per degree. This may be an inappropriate meridional resolution, as exemplified by the differences found between the analysis and mooring records (cf. appendix B).

At the equator we also find at 300 db a seasonal cycle of the currents relative to 400 db (at 10°W, minimum in the early part of the year), but the uncertainty is very large, and the approximations made are questionable. Several years long time series of currents from moorings would be required to improve our understanding of the deep seasonal dynamics. This would allow one to better define the partition between kinetic and potential energy, and to investigate the vertical pressure work.

Acknowledgments. The temperature profiles were provided by the TOGA subsurface data centre, at an early stage of its implementation, with the kind help of J. P. Rébert and N. Cloatre. The FOCAL-SEQUAL dataset was compiled by R. Heimerdinger at NODC, and ancillary data were collected from various institutions, which generously made them available to us. We are particularly thankful to J. J. Le Chauve, D. Corre and R. Chuchla of the Centre Informatique ORSTOM in Brest, to the Institut fur Meereskunde in Kiel and to the Alfred-Wegener Institut für Polar Forschung in BremerHaven. The study was initiated by a discussion in 1982 with Thierry Delcroix. Helpful comments were provided by Bob Houghton, Steve Zebiak, Frank Aikman, Christine Duchêne, Sophie Wacongne, Eli Katz, and colleagues from the ORSTOM Centre in Nouméa. Figures were drafted by J. Distrophe.

APPENDIX A

Temperature Data and the *T–S* Relationship

The temperature profiles originate primarily from a TOGA subsurface data center file obtained in June 1988. The 8-year long analysis (May 1980–April 1988) includes 4732 profiles between 16°S and 20°N in the upper thermocline on the western route, and on the eastern route between 11°N and 11°S there are 3050 profiles for the same period. Each month is sampled, except in early 1980 and late in 1982–early 1983 for the western route, and early 1986 and 1982–1983 for the eastern sections, when data have been supplemented from other programs (both, CTDs and XBTs). The number of profiles of sufficient quality decreases below 400 meters (1119 profiles on the western route, and 847 on the eastern route reach 700 m). Meridional sections in previous years (1976–84) are also available along 4°W (CTD casts and a few XBTs), five degrees to the east of the eastern route at the equator. This is the longitude earlier analyzed by Houghton (1983), and it will serve as an independent benchmark for the eastern route.

Large errors, both systematic and random, have been observed in the lower portion of XBT profiles (Heinmiller et al. 1983). We have not corrected profiles from these expected systematic errors, and we will not consider T4 XBTs below 400 m, and T7 XBTs below 700 m. Also, some of the profiles are extracted from radio messages of a lower quality, which can result in a temperature noise larger than 0.10°C. Together with aliasing of subseasonal time scales and the variability associated with steplike features in the temperature profiles, a large rms is found below 200 meters, both for temperature at a given depth or isotherm depths. For example, at 3°N on the western route, the subseasonal rms variability exceeds 20 meters for the depth of the 11°C isotherm (nominally 300 meters), while it is of the order of 8 meters for the 20°C isotherm (centered at 90 meters depth). This large rms variability does induce an error on the analysis of the seasonal scales.

To reconstruct the low frequency variability, time series in spatial bins are obtained with an objective fitting of the data onto specified functions. These functions are sine and cosine of a Fourier decomposition with a cutoff at three months period. Following Davies (1985), no expected energy level of the seasonal signal is specified in the algorithm adapted from Bretherton et al. (1984). A first run is performed, where outliers are checked and the erroneous profiles are eliminated. Then, the analysis is run a second time. The percentage of rejection is less than 2% for the XBTs transmitted by the data centers, but it is larger for the radio-message XBTs. Analyzed parameters include isotherm depths and temperature at standard levels.

To estimate dynamic height, we associate a *T–S* relationship to the observed temperature profile. The relation between T and S is estimated primarily from CTD casts in 1982 to 1984 with a meridional resolution of 0.5° to 1°, except north of 14°N where climatology is used. Errors in the salinity can yield substantial variations in the dynamic height and in the deduced geostrophic currents. For example, on the large scale, if we were neglecting meridional changes of salinity (the same *T–S* everywhere), the mean computed geo-

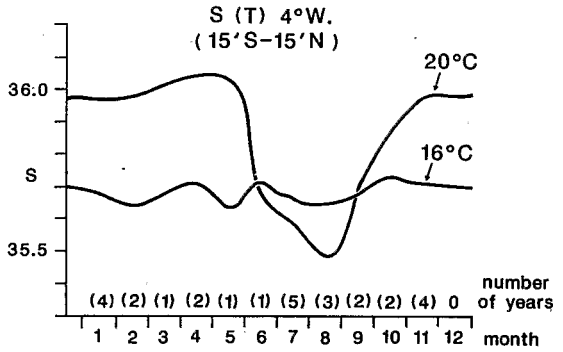

FIG. A1. Near equatorial average seasonal cycle of salinity at 4°W for two temperatures from various CTD casts collected between 1969 and 1984 within 0.25° of the equator. The number of years with data is indicated for each month. There were no profiles in December, which is interpolated between November and January.

strophic currents would change approximately by one-third at 6°N. There are also changes over short distances, which can have a strong influence, for example close to the equator. Arnault (1984) suggests that there is no significant variability of the T–S relationship below 16°C at a specific site off Abidjan at 4°W, 5°N. Above 16°C, there is often a large seasonal cycle in the T–S relationship. It is largest close to the equator in the east (Merle 1978). For instance, in the core of the upper thermocline at (0°, 4°W) (Fig. A1), the seasonal changes in salinity is close to 0.4, and corresponds to a variability in surface dynamic height with a maximum amplitude larger than 1 cm at the equator. We will therefore retain a simplified seasonal cycle above 16°C in the upper thermocline (four seasons: January–March, April–May, June–August, September–December), based on the 1982–84 data with a 0.5° meridional resolution.

APPENDIX B

Estimated Geostrophic Currents; Comparison with Current Meter Moorings in 1983–84

1. Geostrophic currents

We will only comment on the estimation of the zonal velocity component. We can write the meridional momentum equation as: $\beta yu = -\rho^{-1}P_y + A$ (we do not have the data on hand to estimate the terms in A). The horizontal pressure forces are estimated with dynamic height computed from the density with the hydrostatic approximation. Errors in the gridded dynamic height due to an inaccurate T–S relationship (for example, at 6°S) should result in large errors for the mean structure, but not so much for the seasonal fluctuations.

Following various authors (Tsuchiya 1955; Hayes 1982; Lukas and Firing 1984; Johnson et al. 1988),

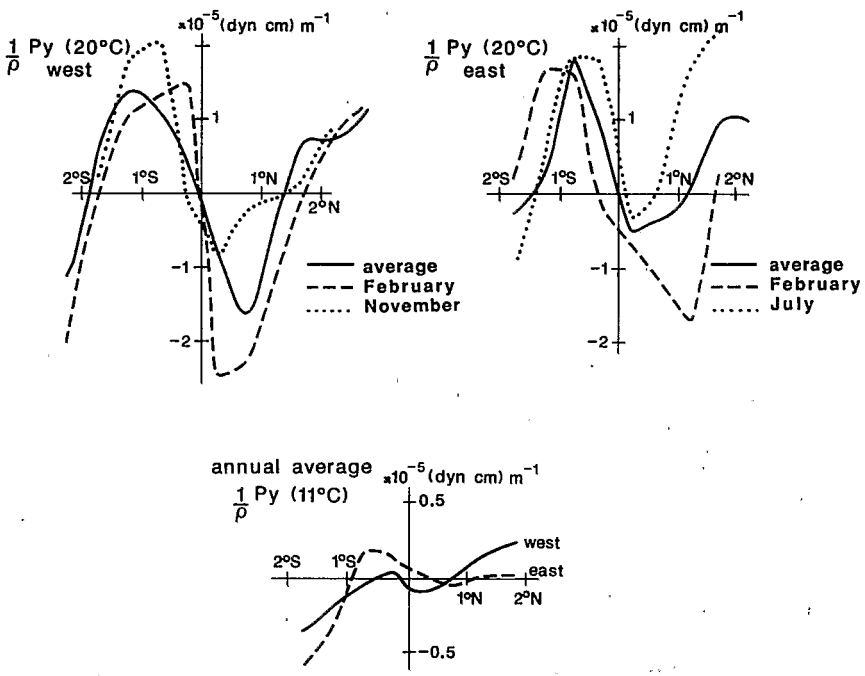

FIG. B1. Meridional profiles of the meridional pressure gradient close to the equator from the 0.5° grid analysis. At the 20°C depth, the average and two extreme situations are shown for the western section (B1a) and the eastern section (B1b). The average is also presented at the 11°C depth for the two sections (B1c) with the vertical scale doubled.

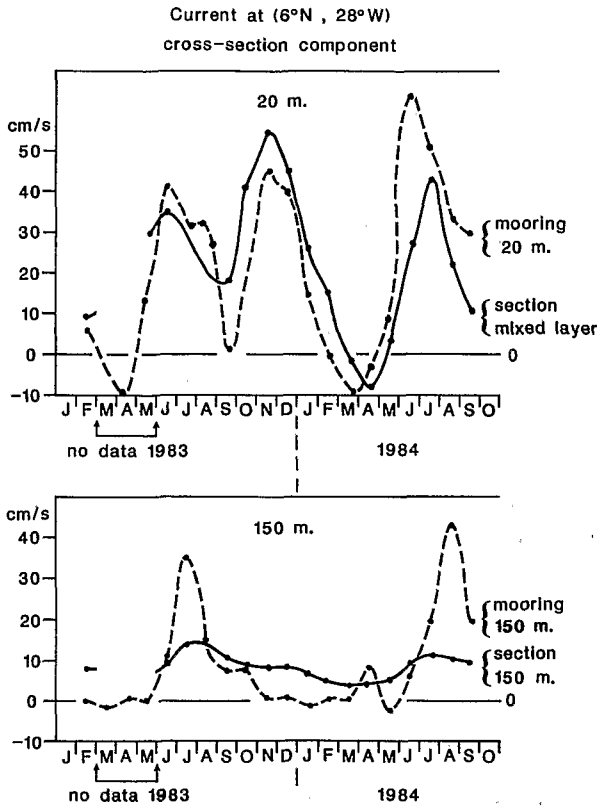

FIG. B2. (Top) Moored current meter measurements at 6°N, 28°W and 20 m (dashed line) compared with the western section analysis at 6°N (full line: here the sum of the geostrophic component and an Ekman component). Only the cross section component is presented. In March–May 1983 there were no XBT profiles.

FIG. B3. (Bottom) Moored current meter measurements at 6°N, 28°W and 150 m (dashed line) compared with the western section analysis at 6°N (full line). Only the cross section component is presented. In March–May 1983 there were no XBT profiles.

an equatorial zonal geostrophic velocity can be estimated from the second derivative of pressure P_{yy} between 1°N and 1°S, as

$$u_g = -1/_{(\rho\beta)} P_{yy}.$$

This corresponds to the current in the ideal case where $A_y = 0$ at the equator. Indeed, near the equator P_y changes sign (Fig. B1), and this condition could be fulfilled. The short meridional scale found on the P_y meridional profile suggests that P_{yy} should be estimated with a 0.5° resolution, and that it will be very uncertain (i.e., in the upper thermocline the value of P_y for a given month has at least a factor of 2 uncertainty). In this respect, the estimates of geostrophic velocity at the equator are not easy to obtain, contrasting with the Pacific Ocean, where the equatorial undercurrent (EUC) is broader, and currents are more symmetric (compare the profiles in Fig. B1 with the sections of Hayes 1982). At the equator P_y can also be significantly nonzero in a given month (for example, the July profiles along the eastern section in Fig. B1b). Other terms in the meridional momentum equation have to be important on a monthly basis, and we can therefore expect that the currents will differ there from the geostrophic currents. Below 150 meters, for example at a temperature of 11°C (Fig. B1c), P_y is very small at the equator, but a small meridional scale (less than 1°) is also found on the P_y profile, an unexpected and unwelcome feature. Therefore, the uncertainty on the equatorial currents relative to 400 db is also expected to be large at depth.

Practically, the sections are not meridional, but oblique, and the along-section pressure gradient may differ from P_y needed to estimate zonal velocity. The magnitude of P_x estimated between the two sections suggests that this effect can reach 10%. Of course, there are places where differences are larger, for instance south of 3°S on the eastern section (the veins of currents have a meridional slant in Mazeika 1968), north of 7°N on the western section below the upper thermocline (Cochrane et al. 1979), and close to the coasts where geostrophic currents are expected to have a significant meridional component. At the equator, P_{yyy} is required to estimate geostrophic currents, and there too the effect due to the slant is likely to reach 10%.

2. Comparison with measured currents

One mooring site at (6°N, 28°W) with current meters at 20 m, 75 m and 150 m between February 1983 and September 1984 is very close to the western XBT section. This provides an opportunity to compare a time series of currents with our analysis. The mooring is located close to the ridge in isotherm depths in the lower thermocline (see Fig. 1a), and the 1.5 degree resolution analysis is not adequate. Unfortunately, there were not enough data on the 0.5° grid to deduce useful time series, and we were obliged to estimate the time series on a 1° grid, so that currents at 6°N are computed between the grid box centered at 5.5°N and the grid box centered at 6.5°N. In the surface layer, to compare with the current records, we add an Ekman

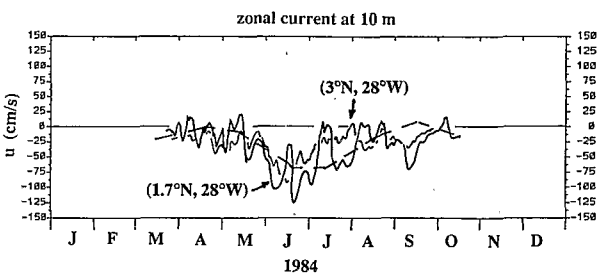

FIG. B4. The two curves are three-day averages 10 m zonal current in 1984 from the two moorings at 3°N and 1.7°N along 28°W. The dashed line corresponds to the analysed current at (2.30°N, 30°W) as the sum of the 1.5° gridded geostrophic analyzed current and an Ekman drift.

velocity uniformly distributed over the mixed layer depth, estimated from the monthly wind stress compiled from ship reports in 1982–84.

The mooring records are presented in Richardson and Reverdin (1987), which suggest that meridional velocities are important on a monthly basis. The cross-section velocity includes a contribution from both zonal and meridional velocity components. At the depth of 20 m, the meridional velocity contribution to the monthly cross-line transport has a rms of 5.4 cm s^{-1}, as the zonal component contributes to a rms of 16.8 cm s^{-1}. The comparison between this ground truth and our analysis does not always show a close agreement (Fig. B2). At 20 m, there is a very large difference in 1984 (especially in June 1984) when the mooring currents are much larger. However, buoy drifts between 5°N and 10°N also indicated that the currents were lower in 1984 compared to 1983 (Richardson and Reverdin 1987). This suggests that the large values observed by the mooring in June and July 1984 may have a meridional scale of the order of 1° or less, which cannot be sensed in our analysis. At 150 m (Fig. B3), there is only a hint of a seasonal cycle in the geostrophic analysis from the XBTs, while the moored currents indicate during the two seasonal cycles an intense eastward pulse of short duration (a little over 2 months). As the moored currents were much weaker at 300 m, the discrepancy cannot be attributed to the reference level. It is possible that these rapidly evolving currents are not well sampled by the XBTs. But it may also be that the mooring was located close to the weakly shifting boundary of a sharp-edged current, and that the analysis smooths this structure too much.

Along 28°W, there were two other moorings at 1°44′N and 3°N for 5 months in 1984. They are a little farther from the XBT track (Fig. 2). The average between the two records can be compared with the 1.5° analysis where the current is estimated between 1°30′N and 3°N (Fig. B4). At the surface, our analysis captures some of the changes, such as the westward pulse in May–June. The magnitude is correct, and differences are comparable to the ones at 6°N. At subsurface, the agreement is not good (not shown). Here, too, it is possible that the analysis smooths too much meridionally the narrow currents (Fig. 9b).

APPENDIX C

Dynamic Height and Acoustical Travel Time

We have seen for the location (0°, 30°W) that the seasonal variability of temperature between 400 m and 700 m (Fig. 8) did induce a peak-to-peak signal of 0.9 dyn cm, compared to a 5 dyn cm peak-to-peak signal between 0 and 400 db. Although the 400 to 700 m layer may contribute only to a fraction of the deep ocean signal, we will illustrate with this layer how the deep ocean variability could be the cause for a less than perfect correlation between surface dynamic height and bottom to surface acoustical travel time from inverted echosounders (IES) (a scaling analysis is also presented in Cartwright et al. 1987). The importance of this analysis is that the signal from inverted echo sounders (IES) placed on the floor of the ocean to measure two-way travel times between the instrument and the ocean surface is usually expected to be an adequate proxi for dynamic height (Katz et al. 1986). An impressive array of IES was implemented in the equatorial Atlantic for the SEQUAL program in 1983–84. Three IES are close to the two routes studied (at 3°N and 9°N, along 28°W, and at 0°, 10°W), and have been presented in Katz (1987) and Garzoli (1987).

Near the equator along the western section, the dynamic height and heat content seasonal cycles for the layer 400–700 db relate well to the temperature measured at 500 m (0.3°C induced a dynamic height signal of 0.9 dyn cm and a travel time signal of 0.4×10^{-3} s), and we applied this relationship to the two sections when there were not enough profiles reaching 700 db. A comparison with acoustical travel time from IES would have been helpful, but there were not enough data at 500 m during these records, and we will only show the estimated average seasonal cycle at two of the sites of the IES measurements. The 300 meter deep

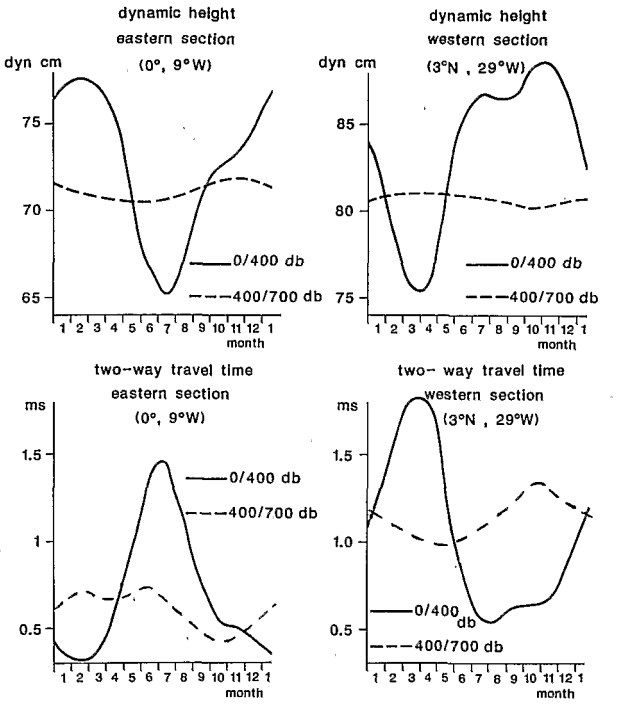

FIG. C1. An estimated two-way travel time in the upper ocean as it would be sensed by an inverted echo sounder. Two locations are presented where an IES was located in 1983–84. The full line depicts the contribution of the top 400 m, and the dashed line is the amplitude of a deeper signal between 400 and 700 m (relative scale).

FIG. C2. As in Fig. C1, but for dynamic height.

layer contributes to about 1 dyn cm and 0.3 ms. Its importance relative to the upper 400 m is much larger in the travel time than in the dynamic height (a factor of 3) (Figs. C1 and C2). This is because sound speed dependency on temperature increases when temperature decreases.

The contribution from the deep layers to travel time can noticeably modify the signal where the deep variability is not in phase with the upper thermocline. In particular, at the equator on the eastern section, if we consider that the travel time is the sum of the contribution of the two layers, there would be less variability between October and March than for the 0–400 m layer alone, and there would be no dip in February.

REFERENCES

Arnault, S., 1984: Variation saisonnière de la topographie dynamique et de la circulation superficielle de l'océan Atlantique tropical. Thèse de doctorat de 3ème cycle, Université Pierre et Marie Curie, Paris.

Bretherton, P., M. McPhaden and E. Kraus, 1984: Design studies for climatological measurements of heat storage. *J. Phys. Oceanogr.*, **14,** 318–337.

Bruce, J. G., J. L. Kerling and W. H. Beatty III, 1985: On the North Brazilian eddy field. *Progress in Oceanography,* Vol. 14, Pergamon, 57–63.

——, 1987: XBT observations between 10°N–10°S in the Atlantic from ship-of-opportunity complemented by XBT surveys. Woods Hole Oceanog. Inst., Tech. Rept. WHOI-87-41.

Busalacchi, T., and J. Picaut, 1983: Seasonal variability from a model of the tropical Atlantic Ocean. *J. Phys. Oceanogr.*, **13,** 1564–1588.

Cane, M., and E. Sarachik, 1981: The response of a linear baroclinic equatorial ocean to periodic forcing. *J. Mar. Res.*, **39,** 651–693.

Cartwright, D. E., R. Spencer and J. M. Vassie, 1987: Pressure variations of the Atlantic equator. *J. Geophys. Res.*, **92,** 725–741.

Cochrane, J. D., F. J. Kelly and C. R. Olling, 1979: Subthermocline countercurrents in the western equatorial Atlantic Ocean. *J. Phys. Oceanogr.*, **9,** 724–738.

Davies, R., 1985: Objective mapping by least square fitting. *J. Geophys. Res.*, **90,** 4773–4777.

Emery, W., W. Zenk, K. Huber, P. Rual and P. Nowlan, 1987: Trends in Atlantic equatorial variability. *Dtsch. Hydrogr. Z.* **40,** 261–276.

Garzoli, S. L., 1987: Forced oscillations on the equatorial Atlantic basin during the seasonal response of the equatorial Atlantic program (1983–1984). *J. Geophys. Res.*, **92,** 5089–5100.

——, and E. J. Katz, 1983: The forced annual reversal of the Atlantic north equatorial countercurrent. *J. Phys. Oceanogr.*, **13,** 2082–2090.

Hayes, S. P., 1982: A comparison of geostrophic and measured velocities in the equatorial undercurrent, *J. Mar. Res.*, **40**(Suppl), 219–229.

Heinmiller, R., C. Ebbesmeyer, B. Taft, D. Olson and O. Nikitin, 1983: Systematic errors in expandable bathythermograph (XBT) profiles. *Deep-Sea Res.*, **30,** 1185–1196.

Hisard, P., and C. Hénin, 1987: Response of the equatorial Atlantic ocean to the 1983–1984 wind from the Programme Français Océan et Climat dans l'Atlantique équatorial cruise data set. *J. Geophys. Res.*, **92,** 3759–3768.

Houghton, R. W., 1983: Seasonal variations of the subsurface thermal structure in the Gulf of Guinea. *J. Phys. Oceanogr.*, **13,** 2070–2081.

——, and C. Colin, 1986: Thermal structure along 4°W in the Gulf of Guinea during 1983–1984. *J. Geophys. Res.*, **91,** 11 727–11 739.

Johnson, E. S., L. A. Regier and R. Knox, 1988: A study of geostrophy in tropical Pacific Ocean currents during the NORPAX Tahiti shuttle using a shipboard Doppler acoustic current profiler. *J. Phys. Oceanogr.*, **18,** 708–723.

Katz, E., 1981: Dynamic topography of the sea surface in the equatorial Atlantic. *J. Geophys. Res.*, **92,** 1885–1893.

——, 1987: Seasonal response of the sea surface to the wind in the equatorial Atlantic. *J. Geophys. Res.*, **92,** 1885–1893.

——, and S. L. Garzoli, 1982: Response of the western equatorial Atlantic Ocean to an annual wind cycle. *J. Mar. Res.*, **40,** 307–327.

——, P. Hisard, J. M. Verstraete and S. L. Garzoli, 1986: Annual change of sea surface slope along the equator of the Atlantic Ocean in 1983 and 1984. *Nature,* **322,** 245–247.

Lukas, R., and E. Firing, 1984: The geostrophic balance of the Equatorial Undercurrent. *Deep-Sea Res.*, **31,** 61–66.

Mazeika, P. A., 1968: Eastward flow within the south equatorial current in the eastern south Atlantic. *J. Geophys. Res.*, **73,** 5819–5828.

McCreary, J. P., J. Picaut and D. W. Moore, 1984: Effects of remote forcing in the eastern tropical Atlantic Ocean. *J. Mar. Res.*, **42,** 45–81.

Merle, J., 1978: Atlas hydrologique saisonnier de l'océan Atlantique intertropical. *Travaux et Documents de l'ORSTOM,* **82,** 64 pp.

——, 1980: Seasonal heat budget in the equatorial Atlantic Ocean. *J. Phys. Oceanogr.*, **10,** 464–469.

——, 1983: Seasonal variability of subsurface thermal structure in the tropical Atlantic Ocean. *Hydrodynamics of the Equatorial Ocean,* J. C. Nihoul, Ed., Elsevier, 31–49.

——, and S. Arnault, 1985: Seasonal variability in the tropical south Atlantic Ocean. *J. Mar. Res.*, **43,** 267–288.

Molinari, R., 1982: Observation of eastward currents in the tropical south Atlantic Ocean: 1978–1980. *J. Geophys. Res.*, **87,** 9707–9714.

du Penhoat, Y., and A. M. Tréguier, 1985: The seasonal linear response of the tropical Atlantic Ocean. *J. Phys. Oceanogr.*, **15,** 316–329.

Philander, G. H., and R. Pacanowski, 1986: A model of the seasonal cycle in the tropical Atlantic Ocean. *J. Geophys. Res.*, **91,** 14 192–14 206.

Picaut, J., 1983: Propagation of the seasonal upwelling in the eastern tropical Atlantic. *J. Phys. Oceanogr.*, **13,** 18–37.

Richardson, P., and G. Reverdin, 1987: Seasonal cycle of velocity in the Atlantic North Equatorial Countercurrent as measured by surface drifters, current meters, and ship drifts. *J. Geophys. Res.*, **92,** 3691–3708.

Rual, P., and F. Jarrige, 1984: Tropical Atlantic thermal structures along the Europe–Brazil ship line. *Geophys. Res. Lett.*, **11,** 775–778.

Stramma, L., and G. Siedler, 1988: Seasonal changes in the North Atlantic subtropical gyre. *J. Geophys. Res.*, **93,** 8111–8118.

Tsuchiya, M., 1955: On a simple method of estimating the current velocity at the equator. *J. Oceanogr. Soc. Japan,* **11,** 1–4.

Weisberg, R. H., 1985: Equatorial Atlantic velocity and temperature observations. February–November 1981. *J. Phys. Oceanogr.*, **15,** 533–543.

——, and A. M. Horigan, 1981: Low frequency variability in the equatorial Atlantic. *J. Phys. Oceanogr.*, **11,** 913–920.

——, and T. J. Weingartner, 1986: On the baroclinic response of the zonal pressure gradient in the equatorial Atlantic Ocean. *J. Geophys. Res.*, **91,** 11 717–11 725

——, and T. Y. Tang, 1987: Further studies on the response of the equatorial thermocline in the Atlantic Ocean to the seasonally varying trade winds. *J. Geophys. Res.*, **92,** 3709–3727.

——, J. H. Hickman, T. Y. Tang and T. J. Weingartner, 1987: Velocity and temperature observations during the seasonal response of the equatorial Atlantic Experiment at 0°, 28°W. *J. Geophys. Res.*, **92,** 5061–5075.